Hindawi
International Journal of RF and Microwave Computer-Aided Engineering
Volume 2024, Article ID 6662753, 9 pages
https://doi.org/10.1155/2024/6662753

Research Article

A Lumped-Element Directional Coupler for Bandwidth Enhancement, Impedance Matching, and Harmonic Suppressions

Murong Zhuo

School of Integrated Circuits, Beijing University of Posts and Telecommunications, Beijing 100876, China

Correspondence should be addressed to Murong Zhuo; zhuomurong@gmail.com

Received 9 June 2023; Revised 24 January 2024; Accepted 27 January 2024; Published 22 February 2024

Academic Editor: Guoan Wang

Copyright © 2024 Murong Zhuo. This is an open access article distributed under the Creative Commons Attribution License, which permits unrestricted use, distribution, and reproduction in any medium, provided the original work is properly cited.

This paper presents a lumped-element wideband directional coupler that enables arbitrary impedance matching and harmonic suppressions from $2f_0$. The coupler consists of four filtering networks (FNs) and an asymmetric branch-line hybrid serving as the matching network. The use of lumped-element topology helps reduce circuit size and improve harmonic suppressions. Each FN, composed of two lumped-element resonators, contributes two additional transmission poles, enabling bandwidth scaling, bandwidth enhancement, and harmonic suppressions. To demonstrate the effectiveness of the proposed design, a wideband coupler with various terminal impedances operating at 0.5 GHz is designed, simulated, and fabricated. The measured size is $0.039 \times 0.039\ \lambda_g^2$, the fractional bandwidth for −14.3 dB return loss is 46%, and the harmonic suppression is more than −30 dB from 0.69 to 4.5 GHz.

1. Introduction

Directional couplers are essential components in wireless communication systems as they provide power division with proper phase differences between two outputs. However, traditional branch-line couplers, comprising four 90° transmission-line sections (TLs), suffer from drawbacks such as large circuit space occupation and high-order harmonics that can interfere with other devices. To mitigate these issues, additional low-pass filters are often used to eliminate unwanted harmonics. Previous attempts have been made to address these challenges using combinations of TLs and inductors [1], parallel-shorted and open stubs [2], parallel TLs [3], dual-open/short-stub loaded resonator [4, 5], coupled lines [6], and lumped-element topologies [7]. However, these approaches have only achieved narrow harmonic-suppression bandwidths, limiting their practical applications.

There have been extensive researches on multifunctional multiport components in recent literatures [1–18]. This is because cascading multiple microwave components can lead to increased circuit area, fabrication complexity, and insertion loss in the radio frequency front end. These components have been studied for various applications such as dual/multiband performance [8–13], wideband filtering performance [14, 15], and arbitrary impedance matching [16–18]. However, the couplers proposed in [8–16], which are based on microstrip-line structures, are limited by their large circuit sizes. On the other hand, in [17, 18], lumped-element couplers with real/complex impedance matching are only suitable for narrow bands due to their low fractional bandwidths.

In recent years, there has been a growing need for miniaturization and bandwidth extension in modern wireless communication systems. To achieve a reduction in circuit size, the composite right-left handed (CRLH) unit is utilized to replace traditional transmission line (TL) branches, as demonstrated in articles [19, 20]. Ultraminiaturized wideband bandstop filters and miniaturized wideband bandpass filters with frequency-dependent complex source and load have been realized using integrated passive devices (IPD) technology in [21, 22]. Additionally, an ultraminiaturized wideband power divider utilizing generalized quasi-Chebyshev and -elliptic low-pass filtering networks has been reported in [23].

In this paper, a novel lumped-element coupler, as shown in Figure 1(a), is proposed. It is equivalent to a traditional

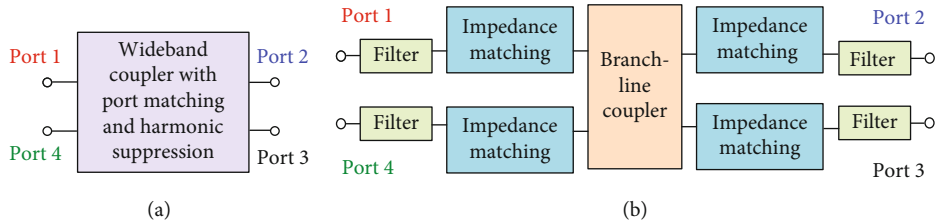

FIGURE 1: Diagrams of the proposed lumped-element coupler. (a) The proposed diagram and (b) its equivalent circuit structure.

branch-line coupler, four impedance matching network, and four filters as depicted in Figure 1(b). The coupler is synthesized using an asymmetric branch-line hybrid and designed filtering networks (FNs). The filtering networks provide variable bandwidths, which are controlled by a bandwidth control factor described in Section 2.3. In this study, a circuit-based simulation using the schematic feature of the Advanced Design System (ADS) software was employed in Section 2, while a full-wave simulation utilizing the Momentum simulation in microwave mode of ADS software was conducted in Section 4. This design theory addresses the common impedance mismatch in circuits by integrating impedance matching, eliminating the need for additional circuits and thereby reducing design complexity and losses. While primarily for theoretical validation at 0.5 GHz, this work can operate across various frequencies and is applicable in fields like the Beidou System and satellite telephony. To the best of the authors' knowledge, there are only a few previous works that have focused on branch-line couplers with wideband, controllable bandwidth, compact size, wideband harmonic suppressions, and arbitrary impedance matching.

2. Analysis of the Proposed Coupler

Figure 2 shows the schematic of the proposed lumped-element wideband coupler for arbitrary impedance matching and harmonic suppressions. This proposed coupler essentially consists of four sets of filtering networks (FNs) and a matching network (MN).

2.1. Matching Network. The matching network is a conventional asymmetric branch-line hybrid for performing coupling and impedance matching. According to [17], when the phase difference is set at 90°, the $Y-$matrix of the matching network can be synthesized as follows:

$$Y = j \times \begin{pmatrix} 0 & \frac{\sqrt{2}}{\sqrt{R_1 R_2}} & 0 & \frac{1}{\sqrt{R_1 R_4}} \\ \frac{\sqrt{2}}{\sqrt{R_1 R_2}} & 0 & \frac{1}{\sqrt{R_2 R_3}} & 0 \\ 0 & \frac{1}{\sqrt{R_2 R_3}} & 0 & \frac{\sqrt{2}}{\sqrt{R_3 R_4}} \\ \frac{1}{\sqrt{R_1 R_4}} & 0 & \frac{\sqrt{2}}{\sqrt{R_3 R_4}} & 0 \end{pmatrix}, \quad (1)$$

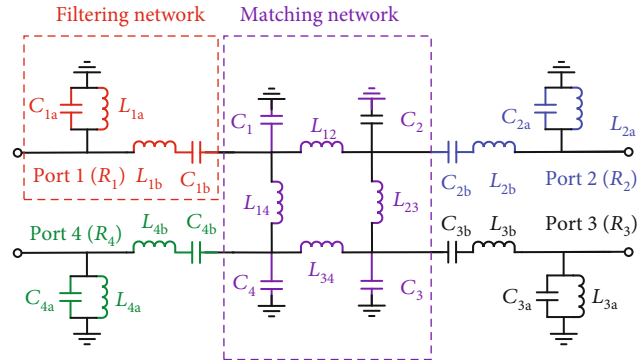

FIGURE 2: Schematic of the proposed coupler.

where R_1, R_2, R_3, and R_4 are the terminal impedances of the four ports and set at 50, 60, 70, and 100 Ω, respectively. Figure 3 shows two types of asymmetric branch-line couplers, one composed of transmission-line sections and the other consisting of lumped elements.

For convenience, the electrical length (θ) is set at 90° at the center frequency f_0. The characteristic impedances Z_{ij} of the conventional transmission-line branch-line hybrid shown in Figure 3(a) can be given as [20]

$$Z_{ij} = \frac{j \csc(\theta)}{Y(i,j)} = \frac{j \csc(\theta)}{Y(j,i)}, \left(\text{where } \frac{i}{j} = 1, 2, 3, 4\right). \quad (2)$$

Similar to the previous one, the lumped-element-based model of the circuit shown in Figure 3(b) consisted of series impedances *Lij* and shunt capacitance *Ci* is [14]

$$\begin{cases} L_{ij} = \dfrac{\mathrm{Im}\left[-(1/Y(i,j))\right]}{2\pi f_0} \\ C_i = \dfrac{\mathrm{Im}\left[\sum_{j=1}^{N=4} Y(i,j)\right]}{2\pi f_0} \end{cases}, \left(\text{where } \frac{i}{j} = 1, 2, 3, 4\right). \quad (3)$$

2.2. Filtering Network. For further improving the harmonic suppressions and expanding the bandwidth, a filtering network composed of a series inductance and capacitance resonator and shunt inductance and capacitance resonators is loaded on the four ports of the matching network.

To achieve the desired functions, including impedance matching and tunable fractional bandwidth (FBW), the four ports are analyzed separately, as shown in Figure 4(a). A portion of the matching network (MN) can be equivalently

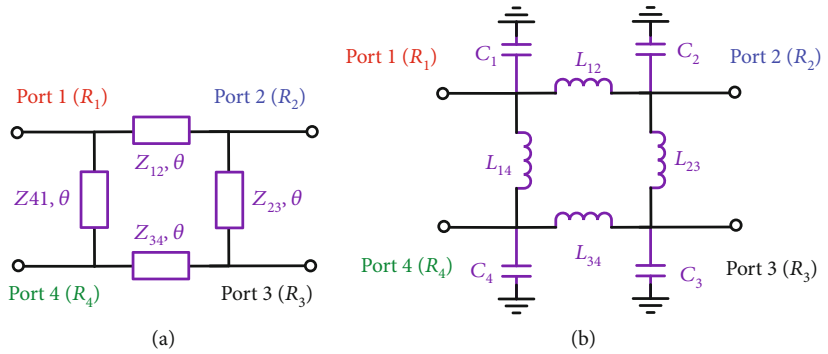

FIGURE 3: Asymmetric branch-line couplers with (a) transmission-line sections and (b) lumped elements.

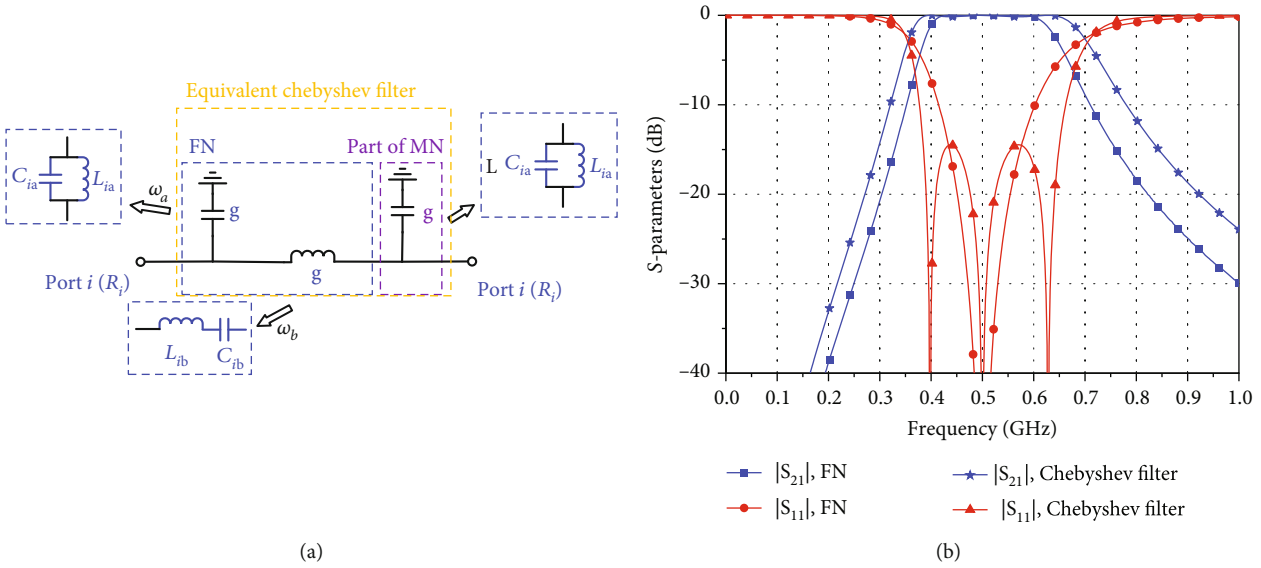

FIGURE 4: (a) Lumped-element circuit schematic of the proposed FN. (b) Ideal simulated S-parameters of the proposed FN and equivalent Chebyshev filter.

represented as a parallel combination of capacitors and inductors, which, when connected in series with the filtering network (FN), forms an equivalent Chebyshev filter. As depicted in Figure 4(b), the FN itself has only one pole. However, when a part of the MN is equivalent to capacitors and inductors similar to those in the FN and then connected in series with it, three poles are achieved.

To obtain an equivalent Chebyshev filter, the inductance L_{ib} and C_{ia} should conform to the criteria outlined in [24]:

$$C_{ia} = \frac{g}{2\pi f_0 B R_i}$$
$$L_{ib} = \frac{g R_i}{2\pi f_0 B}, \quad (4)$$
$$i = 1, 2, 3, 4,$$

where g is the normalized impedance of lumped element, which would affect the return loss and isolation. Here, g is set at 1 for simplification. The B is the bandwidth control factor. According to the port impedance matching ($S_{ii} = 0$, $i = 1, 2, 3, 4$) at the center frequency f_0, L_{ia} and C_{ib} should meet:

$$L_{ia} = \frac{1}{C_{ia}\omega_0^2}, \quad (5)$$

$$C_{ib} = \frac{1}{L_{ib}\omega_0^2}, \quad (6)$$

where $\omega_0 = 2\pi f_0$. Ideal simulated S-parameters of the proposed FN are shown in Figure 4(b), with $R = 50\,\Omega$, $f_0 = 0.5$ GHz, and $B = 0.46$. The circuit performance of three impedance-matching couplers is compared in Figure 5. Its design specifications include $R_1 = 50\,\Omega$, $R_2 = 60\,\Omega$, $R_3 = 75\,\Omega$, $R_4 = 100\,\Omega$, $f_0 = 0.5$ GHz, and $B = 0.46$. From Figure 5, it can be observed that, compared to a coupler implemented with only the matching network (MN), the addition of the filtering network (FN) externally to the MN enables wideband matching, generating two additional transmission points (TPs) and achieving harmonic suppression, thereby enhancing the bandwidth. Furthermore, good harmonic

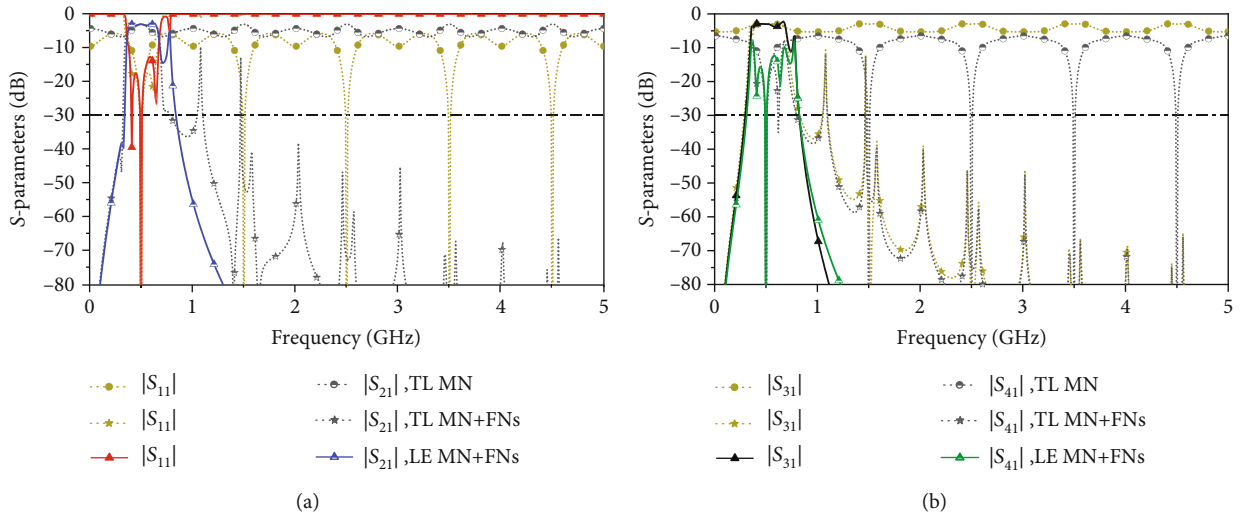

FIGURE 5: Ideal simulated *S*-parameters of (a) $|S_{11}|$ and $|S_{21}|$ and (b) $|S_{31}|$ and $|S_{41}|$ of transmission-line matching network (TL matching network), transmission-line matching network (TL matching network) with FNs, and lumped-element matching network (LE matching network) with FNs.

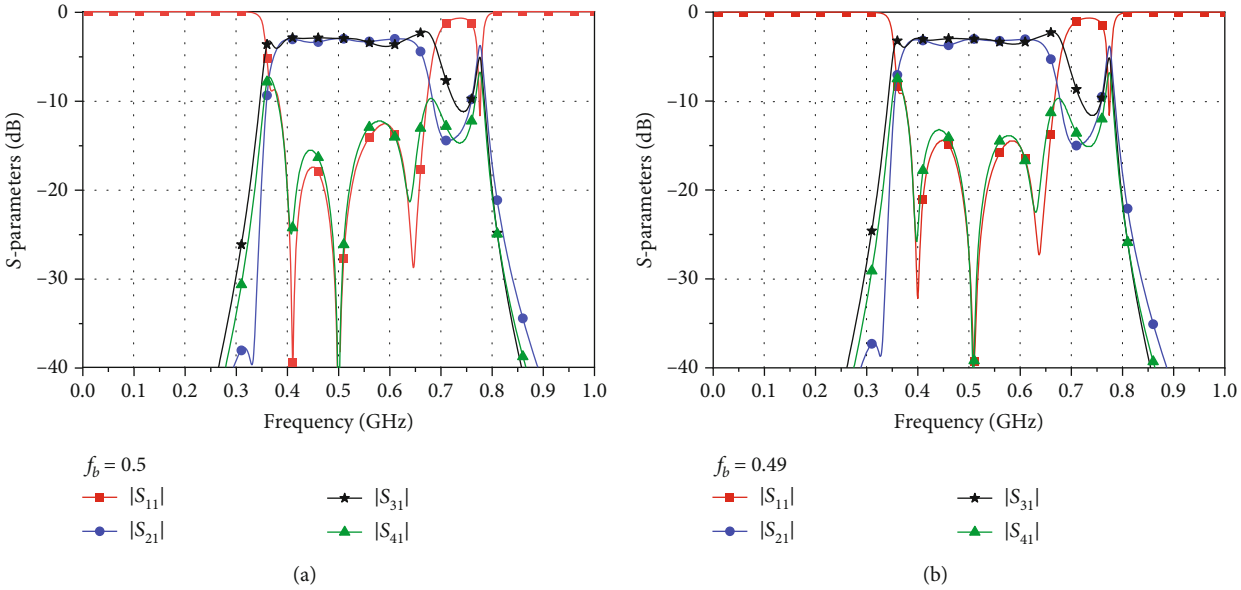

FIGURE 6: Ideal simulated *S*-parameters of the proposed coupler with (a) $f_b = 0.50$ and (b) $f_b = 0.49$.

suppressions from $2f_0$ are obtained when the lumped-element matching network is adopted.

So far, we have synthesized a new coupler with the matching network determined by (1) and (3), and L_{ia}, C_{ia}, L_{ib}, and C_{ib} dominate the FNs according to ((4)–(6)). For both return loss and isolation, the extra two TPs are located at 0.40 and 0.63 GHz when $B = 0.46$. Although the FNs are perfectly matched at the design frequency f_0, the added TPs are not perfectly matched, as shown in Figure 6(a). Rewrite the (6) as

$$C_{ib} = \frac{1}{L_{ib}\omega_0^2}, \tag{7}$$

where $\omega_b = 2\pi f_b$. As shown in Figure 6(b), the value of f_b can change the level of return loss and isolation. Therefore, tuning the value of f_b can realize better return loss and higher isolation for the proposed coupler. Based on equations ((1)–(7)), the lumped-element parameters in Figure 2 are calculated and listed in Tables 1 and 2.

*2.3. The Bandwidth Control Factor (**B**).* The ideal simulated *S*-parameters of the proposed coupler for various *B* are shown in Figure 7. For both return loss and isolation, it can be seen that the extra two TPs are located at 0.40 and 0.61 when $B = 0.4$. When $B = 0.5$, the extra two TPs

Table 1: Parameter, simulation, and measured lumped-element values of the matching network.

	Matching network					
	Pra.	Sim.	Mea.		Pra.	Sim.	Mea.
L_{12} (nH)	12.33	11	11	C_1 (pF)	12.72	12	12
L_{23} (nH)	21.35	20	22	C_2 (pF)	12.96	12	12
L_{34} (nH)	19.17	18	18	C_3 (pF)	9.94	9	8
L_{41} (nH)	22.51	22	24	C_4 (pF)	9.70	9	8

Table 2: Parameter, simulation, and measured lumped-element values of the filtering network.

	Filtering network					
	Pra.	Sim.	Mea.		Pra.	Sim.	Mea.
L_{1a} (nH)	7.32	8.7	8.7	L_{3a} (nH)	10.98	12	12
C_{1a} (pF)	13.84	12	12	C_{3a} (pF)	9.22	8.2	8.2
L_{1b} (nH)	34.60	33	33	L_{3b} (nH)	51.89	51	51
C_{1b} (pF)	3.05	3.1	3.0	C_{3b} (pF)	2.03	1.9	1.9
L_{2a} (nH)	8.78	9.5	9.5	L_{4a} (nH)	14.64	16	16
C_{2a} (pF)	11.53	10	10	C_{4a} (pF)	6.92	6.8	6.8
L_{2b} (nH)	41.52	39	39	L_{4b} (nH)	69.20	68	68
C_{2b} (pF)	2.54	2.5	2.4	C_{4b} (pF)	1.52	1.4	1.4

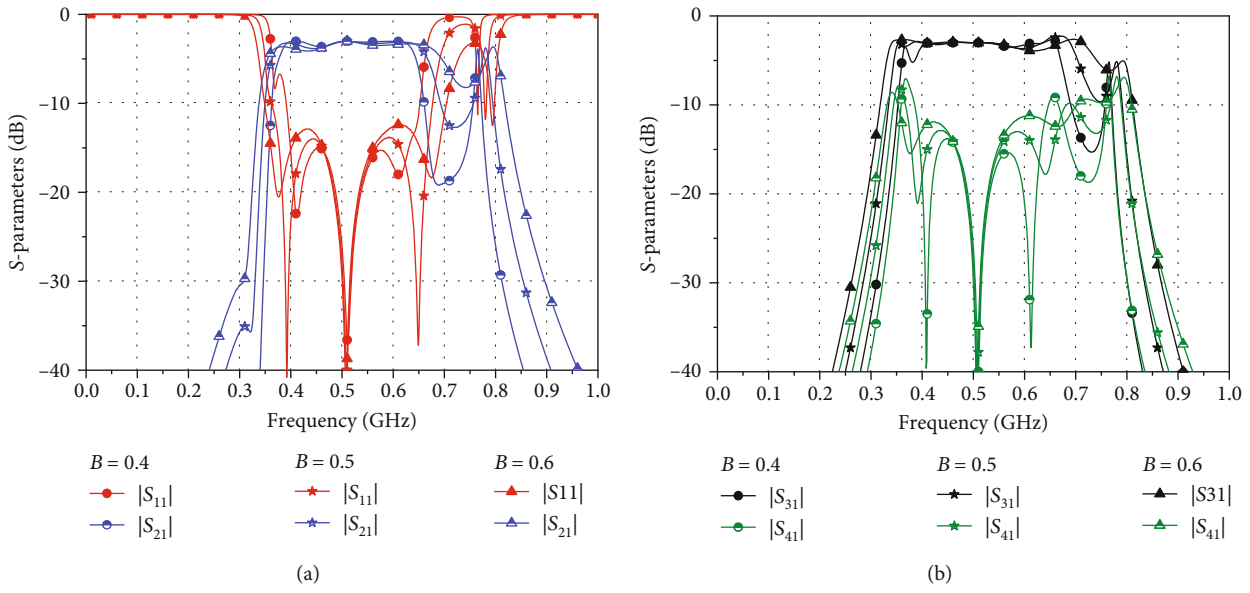

Figure 7: Ideal simulated S-parameters of the proposed coupler for various bandwidth control factors (B) ($f_b = 0.49$). (a) $|S_{11}|$ and $|S_{21}|$. (b) $|S_{31}|$ and $|S_{41}|$.

are located at 0.395 and 0.645. When $B = 0.6$, the extra two TPs are located at 0.375 and 0.675. Thus, it can be calculated that the fractional bandwidths (FBWs) between two transmission poles are 40%, 50%, and 60% at center frequency $f_0 = 0.5$ GHz, respectively, which is equal to the specified values of B.

It can be concluded that, since the value of B is approximately equal to the FBW between the two poles of return loss and isolation, the desired bandwidth can be easily achieved by selecting appropriate B.

3. Design Procedure

In order to provide a clear guidance according to the above analysis, the flow chart is shown in Figure 8, and the design procedure of the proposed lumped-element wideband coupler is summarized as follows:

(1) Specify the desired specifications including the center frequency (f_0) and the terminal impedances (R_1, R_2, R_3, and R_4) of the four ports

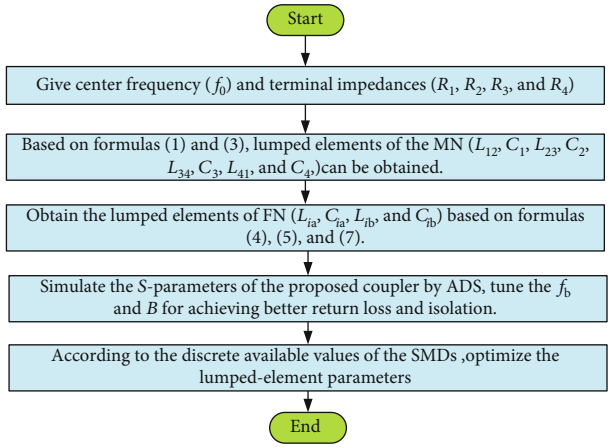

FIGURE 8: Flow chart for the design of the lumped-element coupler.

(2) Then calculate the lumped elements (L_{12}, C_1, L_{23}, C_2, L_{34}, C_3, L_{41}, and C_4) of the matching network using equations (1) and (3).

(3) Select the initial value of B according to the desired bandwidth and calculate the lumped elements of FN (L_{ia}, C_{ia}, L_{ib}, and C_{ib}) based on equations (4), (5), and (7). Construct the circuit model and simulate the S-parameters of the proposed coupler in Figure 2 by the ADS software and tune the f_b for achieving better return loss and isolation. If the specifications cannot be met, please reselect proper B

(4) According to the dimensions and discrete available values of the surface-mounted devices (SMDs) of the lumped inductors and capacitors, build the transmission-line feeding pad and optimize the lumped-element parameters

4. Experimental Validation

To demonstrate the validity of the design theory obtained from the previous analysis, a lumped-element wideband coupler with the design specifications setting as $f_0 = 0.5$ GHz, $k = 1$, $R_1 = 50\,\Omega$, $R_2 = 60\,\Omega$, $R_3 = 75\,\Omega$, $R_4 = 100\,\Omega$, $f_b = 0.49$, and $B = 0.46$ are simulated, manufactured, and measured using RO4350 ($\varepsilon_r = 3.66$, $h = 1.524$ mm) substrates. Ideal simulated S-parameters of the proposed coupler are shown in Figure 6(b). The final layout and the photograph of the fabricated lumped-element coupler are displayed in Figures 9 and 10. The circuit size is 14.5 mm × 14.3 mm.

Figure 11 shows the results of the full-wave simulation and the final measurement. To account for the inevitable tolerance and discrete available values of the SMDs of lumped inductors and capacitors, the design parameters were fine-tuned; however, there is still some small deviation and slight frequency shift (0.2 GHz) between the simulated and measured frequency responses. The simulated and measured values of the proposed coupler are summarized in Tables 1 and 2. In contrast, the performances of the proposed coupler and several state-of-the-art couplers are tabulated in Table 3.

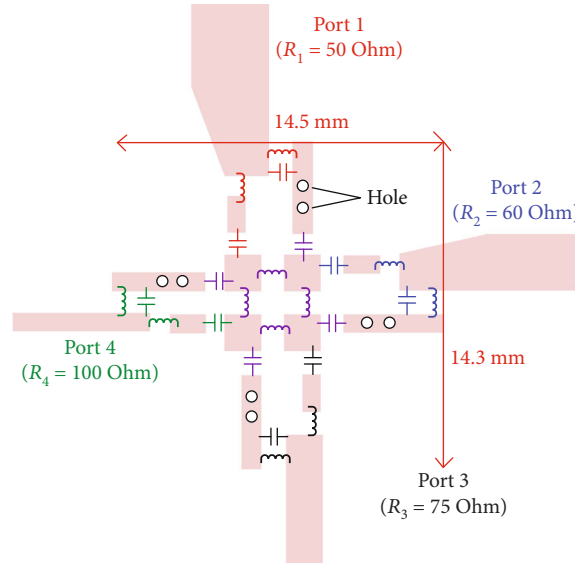

FIGURE 9: Layout of the proposed coupler.

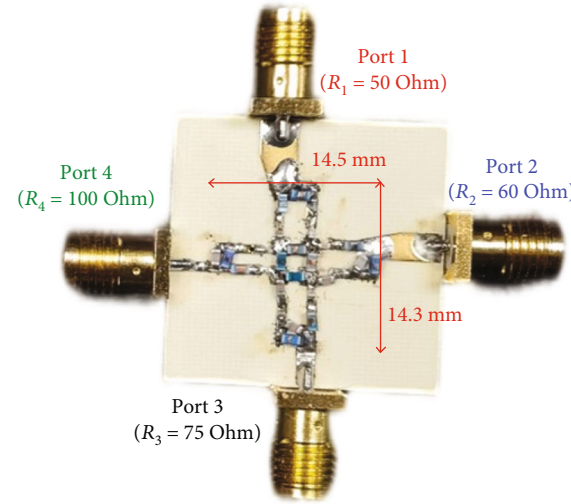

FIGURE 10: Photograph of the proposed coupler.

As shown in Figure 11(a), with the measured center frequency 0.48 GHz, the measured return loss is greater than −14.3 dB from 0.36 to 0.58 GHz, with 46% FBW. The measured insertion losses ($|S_{21}|$ and $|S_{31}|$) are −4.2 dB and −4.4 dB at center frequency, and the maximum amplitude imbalance between Port 2 and Port 3 ($|S_{21}| - |S_{31}|$) of ±1 dB has also been achieved from 0.38 to 0.58 GHz, with 42% FBW. Furthermore, the measured phase difference between Port 2 and Port 3 ($\angle S_{21} - \angle S_{31}$) deviates within ±10° over the range of 3.7 to 6.0 GHz, with 48% FBW. As the $|S_{21}|$ ($|S_{31}|$) and $|S_{12}|$ ($|S_{13}|$) exhibit almost identical characteristics, only the graphs for $|S_{21}|$ and $|S_{31}|$ are displayed. The comparison data shows that it is the first fully lumped-element-based coupler to achieve such bandwidth.

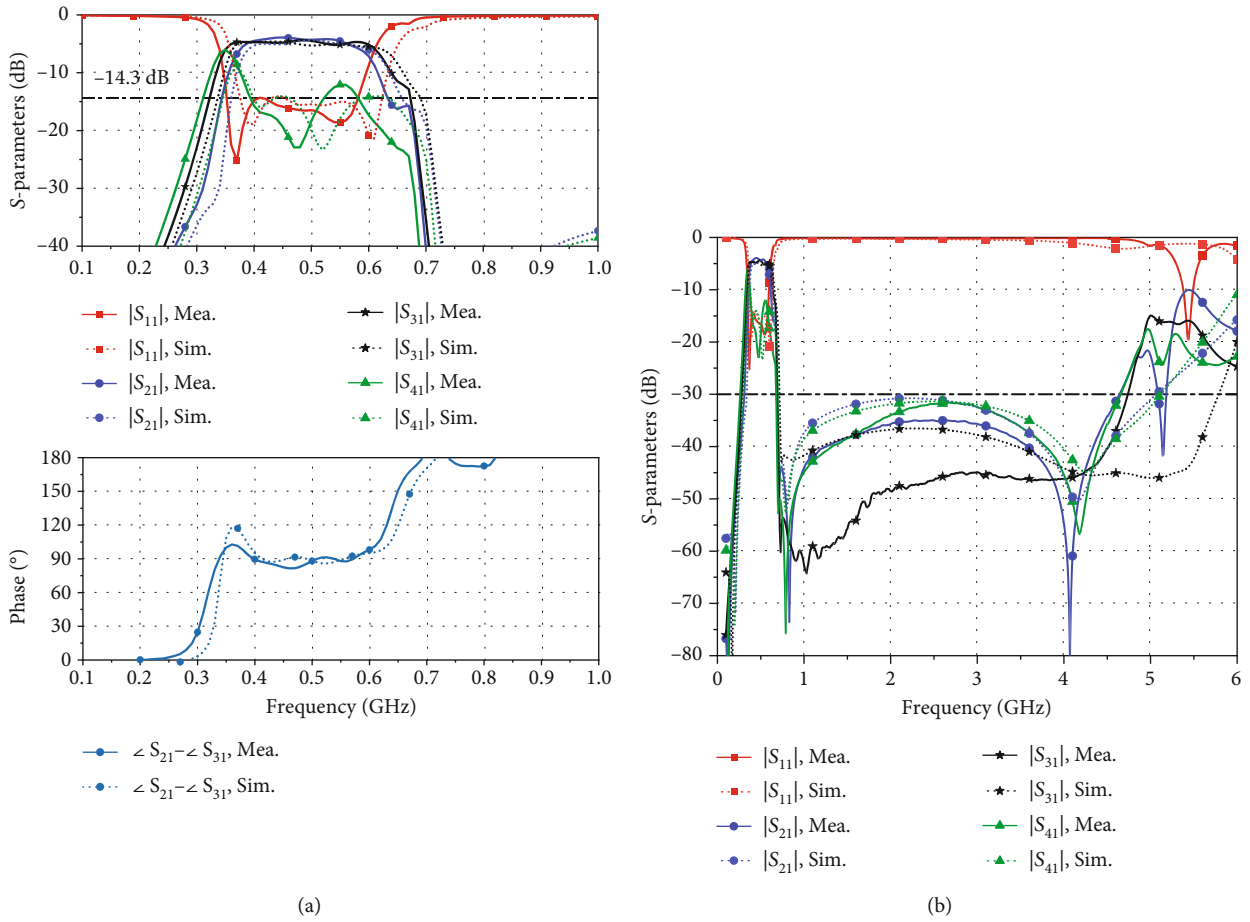

FIGURE 11: EM simulated and measured results of (a) the proposed coupler at $f_0 = 0.5$ GHz and (b) the proposed coupler across a frequency range from 0 to 12 f_0.

TABLE 3: Measured performance comparison with previous works.

Refs.	f_0 (GHz)	FBW (%)/$\|S_{11}\|$ (dB)	PD.	AI.	Harmonic suppression area	Electrical size (λ_g^2)	Technology
[1][1]	1	~50/−15	4 : 1	No	$2f_0 - 4f_0$ (−40 dB)	0.17 × 0.30	Microstrip + SMD
[3]	1	9/−20	1 : 1	No	$2f_0 - 4f_0$ (−15 dB)	0.19 × 0.19	Microstrip
[2]	3	30.5/−15	2.5 : 1-10 : 1	No	$2f_0$ (−15 dB)	0.5 × 0.47	Microstrip
[7][2]	1	4/−15	1 : 1	Yes	X	0.06 × 0.06	SMD
[11]	0.83	38.5/-10	1 : 1	No	$2f_0$ (−20 dB)	0.07 × 0.06	Microstrip
[14]	3.5	61.1/−15	31.6 : 1	No	X	0.39 × 0.84	Microstrip
[12]	1.63/2.73	7.5/5.1[3]	1 : 1	No	$5.2f_1$ (-19.5)	0.25 × 0.25	Microstrip
This work	0.48	46/−14.3	1 : 1	Yes	$2f_0 - 9f_0$ (−30 dB)	0.039 × 0.039	SMD

[1]Prototype II; [2]Case B; [3]3 dB bandwidth. PD.: power division ratio; AI.: arbitrary impedance matching; λ_g: the guided wavelength at the center frequency.

Figure 11(b) illustrates the measured result from 0 to 6 GHz with 0 to −80 dB. Seen that over −30 dB measured harmonic suppressions for insertion loss ($|S_{21}|$ and $|S_{31}|$) and the isolation ($|S_{41}|$) are realized from 0 to 0.26 GHz, and from 0.69 to 4.63 GHz (from $2f_0$ to $9f_0$), respectively. In the ideal model, the resonant zero observed at 0.75 GHz arises from the resonance between capacitors in the MN and inductors in the FN, leading to the noted harmonic. However, the absence of the resonant zero in measurement and EM simulation can be attributed to increased parasitic resistance within the feeding pad and SMDs, which reduces the Q factor, along with the mismatch between commercially available component values and their idealized counterparts used in circuit simulations. This harmonic effect also can potentially be mitigated by optimizing the layout during EM simulations or by refining the MN network.

According to the comparison data, this work uniquely achieves wideband harmonic suppression from $2f_0$ to $9f_0$

with more than −30 dB suppression, while maintaining a remarkably compact size. This achievement is a first in similar designs. Additionally, this work effectively addresses the common issue of narrow bandwidth in lumped-element couplers. Compared to other lumped-element couplers [7], it achieves a tenfold increase in bandwidth and features the capability of arbitrary port impedance. Furthermore, it exhibits significant bandwidth advantages over other structures with the same power distribution ratio and offers flexibility in bandwidth adjustment through parameter tuning. This work achieves a 58% [7] to 99% [14] reduction in electrical size compared to other couplers, indicating its exceptionally compact structure.

The proposed lumped-element coupler theory can reduce PCB size through the application of SMD devices at low frequencies. Additionally, in situations where fabricating transmission lines is impractical, the use of commercial SMD components offers a cost-effective and space-saving solution, while also simplifying the layout optimization process. At high frequencies, the lumped elements can be integrated into chips such as integrated passive devices (IPD) and low-temperature cofired ceramics (LTCC) to reduce the overall area of the chip. Looking ahead, utilizing high-Q (quality factor) SMD components can enhance the circuit's performance, and optimizing the chip layout to achieve the desired values of lumped elements presents a significant challenge.

5. Conclusion

In this paper, for the first time, a fully lumped-element-based coupler with controllable large fractional bandwidth, arbitrary impedance matching, and wideband harmonic suppressions from $2f_0$ has been proposed utilizing MuRata SMDs. Good agreement between EM simulation and measurement demonstrates that the proposed multifunctional coupler is of great potential to reduce the system complexity, circuit size, and fabrication cost of the future RF front-end design.

Data Availability

The data used to support the findings of this study are included within the article.

Conflicts of Interest

The author declares that he has no conflicts of interest.

Acknowledgments

This work is supported by the School of Integrated Circuits, Beijing University of Posts and Telecommunications.

References

[1] H.-R. Ahn and M. M. Tentzeris, "Arbitrary power-division branch-line hybrids for high-performance, wideband, and selective harmonic suppressions from $2f_0$," *IEEE Transactions on Microwave Theory and Techniques*, vol. 67, no. 3, pp. 978–987, 2019.

[2] Z. Qamar, S. Y. Zheng, W. S. Chan, and D. Ho, "Coupling coefficient reconfigurable wideband branch-line coupler topology with harmonic suppression," *IEEE Transactions on Microwave Theory and Techniques*, vol. 66, no. 4, pp. 1912–1920, 2018.

[3] V. K. Velidi, A. V. G. Subramanyam, V. S. Kumar, Y. Mehta, and S. Sanyal, "Compact harmonic suppression branch-line coupler using signal-interference technique," in *2016 Asia-Pacific Microwave Conference (APMC)*, New Delhi, India, 2016.

[4] W. Jiang, T. Wang, Y. Peng, Y. Huang, and G. Wang, "Bandpass filtering power divider with sharp roll-off skirt and enhanced in-band isolation," in *2016 IEEE MTT-S International Microwave Symposium (IMS)*, San Francisco, CA, USA, 2016.

[5] W. Jiang, Y. Huang, T. Wang, Y. Peng, and G. Wang, "Microstrip balanced quad-channel diplexer using dual-open/short-stub loaded resonator," in *2016 IEEE MTT-S International Microwave Symposium (IMS)*, San Francisco, CA, USA, 2016.

[6] D. K. Choudhary and R. K. Chaudhary, "Compact design of filtering branch line coupler for GSM frequencies using coupled TL," in *2021 IEEE MTT-S International Microwave and RF Conference (IMARC)*, KANPUR, India, 2021.

[7] J. Hou and Y. Wang, "Design of compact 90° and 180° couplers with harmonic suppression using lumped-element bandstop resonators," *IEEE Transactions on Microwave Theory and Techniques*, vol. 58, no. 11, pp. 2932–2939, 2010.

[8] Y. Zhang, Y. Wu, W. Wang, Y. Yang, and L. Ma, "Novel multifunctional dual-band coupled-line coupler with reuse of low-frequency trans-directional and high-frequency contra-directional functions," *IEEE Transactions on Circuits and Systems II: Express Briefs*, vol. 68, no. 6, pp. 1917–1921, 2021.

[9] A. M. Zaidi, B. K. Kanaujia, M. T. Beg, J. Kishor, and K. Rambabu, "A novel dual-band branch line coupler for dual-band butler matrix," *IEEE Transactions on Circuits and Systems II: Express Briefs*, vol. 66, no. 12, pp. 1987–1991, 2019.

[10] W. Feng, Y. Zhao, W. Che, H. Chen, and W. Yang, "Dual-/tri-band branch line couplers with high power division isolation using coupled lines," *IEEE Transactions on Circuits and Systems II: Express Briefs*, vol. 65, no. 4, pp. 461–465, 2018.

[11] D. K. Choudhary, N. Mishra, P. K. Singh, and A. Sharma, "Miniaturized power divider with triple-band filtering response using coupled line," *IEEE Access*, vol. 11, pp. 27602–27608, 2023.

[12] J. Ge and G. Wang, "A dual-band filtering structure for highly selective reconfigurable bandpass filter and filtering balun," *International Journal of RF and Microwave Computer-Aided Engineering*, vol. 32, no. 8, article e23215, 2022.

[13] W. Jiang, W. Shen, T. Wang, Y. M. Huang, Y. Peng, and G. Wang, "Compact dual-band filter using open/short stub loaded stepped impedance resonators (OSLSIRs/SSLSIRs)," *IEEE Microwave and Wireless Components Letters*, vol. 26, no. 9, pp. 672–674, 2016.

[14] Y.-N. Zheng, W.-M. Wang, and Y.-L. Wu, "Synthesis of wideband filtering couplers for arbitrary high power-division ratios based on three different types of coupled-line sections," *IEEE Transactions on Circuits and Systems II: Express Briefs*, vol. 68, no. 4, pp. 1218–1222, 2021.

[15] P.-J. Chou, C.-C. Yang, and C.-Y. Chang, "Exact synthesis of unequal power division filtering rat-race ring couplers," *IEEE Transactions on Microwave Theory and Techniques*, vol. 66, no. 7, pp. 3277–3287, 2018.

[16] Y. Wu, L. Jiao, Q. Xue, and Y. Liu, "Reply to comments on 'a universal approach for designing an unequal branch-line coupler with arbitrary phase differences and input/output impedances'," *IEEE Transactions on Components, Packaging and Manufacturing Technology*, vol. 9, no. 6, pp. 1210–1216, 2019.

[17] Z. Chen, Y. Wu, Y. Yang, and W. Wang, "A novel unequal lumped-element coupler with arbitrary phase differences and arbitrary impedance matching," *IEEE Transactions on Circuits and Systems II: Express Briefs*, vol. 69, no. 2, pp. 369–373, 2022.

[18] R. Sinha, "Design of multi-port with desired reference impedances using Y-matrix and matching networks," *IEEE Transactions on Circuits and Systems I: Regular Papers*, vol. 68, no. 5, pp. 2096–2106, 2021.

[19] D. K. Choudhary, "Design of CRLH-TL based compact hybrid coupler loaded with S-shaped slot," in *2021 6th International Conference for Convergence in Technology (I2CT)*, Maharashtra, India, 2021.

[20] D. K. Choudhary and R. K. Chaudhary, "Compact D-CRLH structure for filtering power divider," *Electromagnetics Research Letters*, vol. 94, pp. 93–101, 2020.

[21] M. Kong, Y. Wu, Z. Zhuang, W. Wang, and C. Wang, "Ultra-miniaturized wideband input-absorptive bandstop filter based on TFIPD technology," *IEEE Transactions on Circuits and Systems II: Express Briefs*, vol. 68, no. 7, pp. 2414–2418, 2021.

[22] W. Chen, Y. Wu, Y. Yang, and W. Wang, "IPD-based miniaturized wideband bandpass filter with frequency-dependent complex source and load," *IEEE Transactions on Plasma Science*, vol. 49, no. 3, pp. 1115–1120, 2021.

[23] M. Kong, Y. Wu, Z. Zhuang, W. Wang, and C. Wang, "Ultra-miniaturized wideband quasi-Chebyshev/-elliptic impedance-transforming power divider based on integrated passive device technology," *IEEE Transactions on Plasma Science*, vol. 48, no. 4, pp. 858–866, 2020.

[24] J. S. Hong and M. J. Lancaster, *Microstrip Filter for RF/Microwave Applications*, John Wiley & Sons, New York, NY, USA, 2004.